A Photometric Study of the Contact Binary V737 Cephei

Edward J. Michaels
Stephen F. Austin State University, Department of Physics, Engineering and Astronomy, P.O. Box 13044, Nacogdoches, TX 75962; emichaels@sfasu.edu

Received January 8, 2018; revised January 30, 2018; accepted January 30, 2018

Abstract Presented are the first multiband CCD photometry of the eclipsing binary star V737 Cephei. The observations resulted in 22 new times of minimum. New linear and quadratic ephemerides were computed from all available minimum light timings. The orbital period was found to be rapidly decreasing. The light curves were analyzed with the Wilson-Devinney program to find the best-fit stellar model. The model required a large third-light contribution and a cool spot on the larger star to fit light curve asymmetries. A fill-out of 19% is consistent with a W-subtype contact binary.

1. Introduction

The variability of V737 Cephei (NSV 13695) was first reported by Kukarkin *et al.* (1982). Using photometric observations from the ASAS-3, NSVS, and Hipparcos databases, this star was classified as a W-subtype eclipsing binary with an orbital period of 0.298755 d (Otero *et al.* 2005). Gettel *et al.* (2006) gives a maximum visual magnitude of 11.965 and a minimum of 12.370. The parallax measured from the first data release of the Gaia mission gives a distance of 243 ± 51 pc (Gaia 2016). A total of 17 eclipsing timings were reported by Hübscher *et al.* (2012), Hübscher and Lehmann (2012), Hübscher *et al.* (2013), Hübscher (2013, 2017), Hoňková *et al.* (2013), Nelson (2014, 2016) and Juryšek *et al.* (2017). V737 Cep was included in "The 79th Name-List of Variable Stars" (Kazarovets *et al.* 2008).

Presented in this paper is the first photometric study of V737 Cephei. The photometric observations and data reduction methods are presented in section 2, with new times of minima and ephemerides in section 3. Light curve analysis using the Wilson-Devinney model (WD; Wilson and Devinney 1971) is presented in section 4. A discussion of the results and conclusions are given in section 5.

2. Observations

Multi-band photometric observations were acquired at the Waffelow Creek Observatory (http://obs.ejmj.net/index.php) in July 2015 and July 2017. A 0.30-m telescope was used for the 2015 observations and a 0.36-m telescope in 2017. Both instruments had Ritchey-Chrétien optical systems with a robotic mount for automated observing runs. All images were acquired using a SBIG-STXL camera equipped with a cooled KAF-6303E CCD (–30° C). The 2015 data set was obtained in five passbands: 585 images in Johnson B, 962 in Johnson V, 971 in Sloan g', 756 in Sloan r', and 682 in Sloan i'. The 2017 data set includes 1,183 images in Sloan g', 908 in Sloan r', and 1,247 in Sloan i'. Bias, dark, and flat frames were obtained on each night. MIRA software (Mirametrics 2015) was used for image calibration and to perform the ensemble differential aperture photometry of the light images. The coordinates and magnitudes of the comparison and check stars are listed in Table 1 with a finder chart shown in Figure 1. The standard magnitudes of the comparison stars were taken from the AAVSO Photometric All-Sky Survey (APASS) data base (Henden *et al.* 2014) and were used to convert the instrumental magnitudes of V737 Cep to standard magnitudes. The Heliocentric Julian Date of each observation was converted to orbital phase (ϕ) using the following epoch and orbital period: T_o = 2455685.4877 and P = 0.298765 d. Both the 2015 and 2017 data sets provided new times of minima for V737 Cep. The 2017 observations resulted in complete light curves for each observed passband and were also of higher

Table 1. Stars used in this study.

Star	*R.A. (2000) h m s*	*Dec. (2000) ° ′ ″*	*g′*	*r′*	*i′*
V737 Cep	21 23 48.4	+63 33 28			
[1]GSC 04252-00669 (C1)	21 24 34.5	+63 30 04	11.980	11.445	11.275
[1]GSC 04252-00821 (C2)	21 24 45.6	+63 32 03	12.168	11.580	11.361
[1]GSC 04252-00725 (C3)	21 23 39.3	+63 30 31	13.085	12.004	11.560
[1]GSC 04252-01534 (C4)	21 23 53.1	+63 36 10	12.724	12.044	11.835
[2]GSC 04252-00655 (K)	21 23 41.6	+63 40 07	11.413	11.296	11.320

APASS [1]comparison stars (C1–C4) and [2]check star (K) magnitudes.

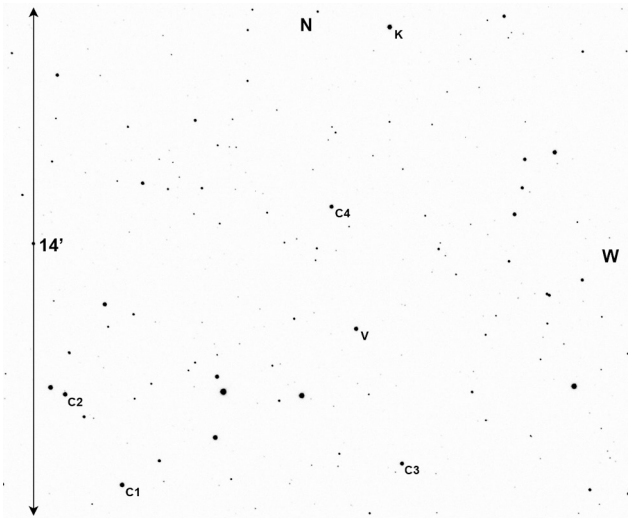

Figure 1. Finder chart for V737 Cep (V), comparison (C1-C4) stars, and check (K) stars.

quality compared to the 2015 data set. This was the result of better seeing conditions in 2017 as well as a higher signal-to-noise ratio provided by the larger telescope. The folded light curves show that both the primary and secondary eclipses are total (Figure 2). All light curves in this paper were plotted from orbital phase –0.6 to 0.6 with negative phase defined as $\phi - 1$. The check star magnitudes were plotted and inspected each night, but no significant variability was noted. The standard deviation of the check star magnitudes (all nights) were 6 mmag for Sloan g', 5 mmag for Sloan r', and 8 mmag for Sloan i'. The Sloan r' check star magnitudes are plotted in the bottom panel of Figure 2. The 2017 observations can be accessed from the AAVSO International Database (Kafka 2017) (https:/www.aavso.org/aavso-international-database).

3. Ephemerides

Table 2 lists 17 times of minima found in the literature along with 22 new minima times from this study. The (O–C) residuals in Table 2 were computed using the following linear ephemeris:

$$\text{HJD Min I} = 2455685.4877 + 0.2987551\text{E}. \quad (1)$$

The epoch for this initial ephemeris uses the first primary minima time shown in Table 2 (Hübscher *et al.* 2012) and the orbital period taken from The International Variable Star Index (VSX; Watson 2006). A new linear ephemeris was computed by least-squares solution using the residuals from Equation 1:

$$\text{HJD Min I} = 2457961.7788(9) + 0.298765(5)\text{E}. \quad (2)$$

Figure 3 shows the residuals of Equation 1 and the best-fit line of Equation 2 (solid line). A second least-squares solution using the Equation 2 residuals yields the following quadratic ephemeris:

$$\text{HJD Min I} = 2457961.7767(7) + 0.298763(5)\text{E} - 3.3(2) \times 10^{-10}\text{E}^2. \quad (3)$$

Figure 4 shows the residuals from Equation 2 and the general trend of the quadratic ephemeris (solid line). The negative curvature indicates a decreasing orbital period, which will be discussed further in section 5.

4. Analysis

4.1. Temperature, spectral type

Pickles and Depagne (2010) using all-sky spectrally matched Tycho 2 stars determined the spectral type of V737 Cep, K0V. A star of this spectral type has an effective temperature of $T_{eff} = 5280$ K and a color of $(B-V)_0 = 0.816$ (Pecaut and Mamajek 2013). To find the observed color, the phase and magnitude of the g' and r' observations were binned with a phase width of 0.01. The phases and magnitudes in each bin interval were averaged. To find the color at quadrature ($\phi = 0.25$), the binned r' magnitudes were subtracted from the linearly interpolated g' magnitudes, giving an observed (g'– r') color of 0.704 ± 0.008. Figure 5 shows the binned r' magnitude light curve with the observed (g'–r') color shown in the bottom panel. The color changes only a small amount over an orbital cycle, which is

Table 2. Times of minima and O-C residuals from Equation 1.

Epoch HJD 2400000+	*Error*	*Cycle*	*O–C*	*References*
55685.4877	0.0006	0.0	0.00000	Hübscher and Lehmann 2012
55692.5070	0.0001	23.5	–0.00148	Hoňková *et al.* 2013
55693.5535	0.0007	27.0	–0.00062	Hoňková *et al.* 2013
55707.4450	0.0001	73.5	–0.00124	Hoňková *et al.* 2013
55787.3664	0.0007	341.0	0.00321	Hübscher and Lehmann 2012
55791.4002	0.0002	354.5	0.00378	Hoňková *et al.* 2013
56072.3892	0.0012	1295.0	0.01365	Hübscher 2013
56072.5405	0.0010	1295.5	0.01557	Hübscher 2013
56421.9450	0.0002	2465.0	0.02598	Nelson 2014
56490.5127	0.0003	2694.5	0.02938	Hübscher 2013
56508.4373	0.0004	2754.5	0.02865	Hoňková *et al.* 2013
56519.3425	0.0002	2791.0	0.02932	Hoňková *et al.* 2013
56519.4923	0.0002	2791.5	0.02973	Hoňková *et al.* 2013
56530.3968	0.0006	2828.0	0.02967	Hoňková *et al.* 2013
57182.8999	0.0001	5012.0	0.05164	Nelson 2016
57217.8561	0.0001	5129.0	0.05345	present paper
57220.8436	0.0001	5139.0	0.05342	present paper
57221.7401	0.0001	5142.0	0.05366	present paper
57222.7864	0.0002	5145.5	0.05436	present paper
57223.8311	0.0001	5149.0	0.05334	present paper
57223.6830	0.0002	5148.5	0.05468	present paper
57224.7273	0.0001	5152.0	0.05327	present paper
57224.8779	0.0002	5152.5	0.05459	present paper
57227.7147	0.0002	5162.0	0.05316	present paper
57227.8652	0.0003	5162.5	0.05428	present paper
57228.7616	0.0002	5165.5	0.05443	present paper
57335.4208	0.0002	5522.5	0.05802	Juryšek 2017
57568.4563	0.0029	6302.5	0.06458	Hübscher 2017
57946.8380	0.0004	7569.0	0.07294	present paper
57952.8131	0.0004	7589.0	0.07291	present paper
57952.6652	0.0004	7588.5	0.07442	present paper
57953.7094	0.0003	7592.0	0.07301	present paper
57953.8602	0.0004	7592.5	0.07442	present paper
57954.7563	0.0002	7595.5	0.07426	present paper
57955.8008	0.0001	7599.0	0.07307	present paper
57955.6525	0.0001	7598.5	0.07418	present paper
57960.8799	0.0001	7616.0	0.07337	present paper
57960.7314	0.0001	7615.5	0.07426	present paper
57961.7762	0.0001	7619.0	0.07343	present paper

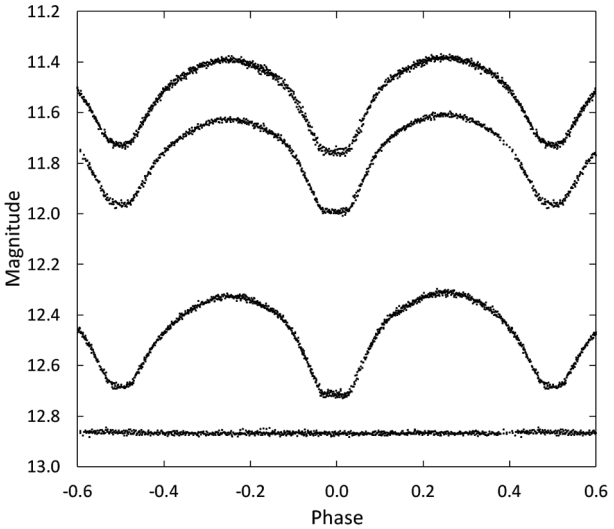

Figure 2. Folded light curves for each observed passband. The differential magnitudes of V737 Cep were converted to standard magnitudes using the calibrated magnitudes of the comparison stars. From top to bottom the light curve passbands are Sloan i', Sloan r', Sloan g'. The bottom curve shows the Sloan r' magnitudes of the check star (offset +1.6 magnitudes). Error bars are not shown for clarity.

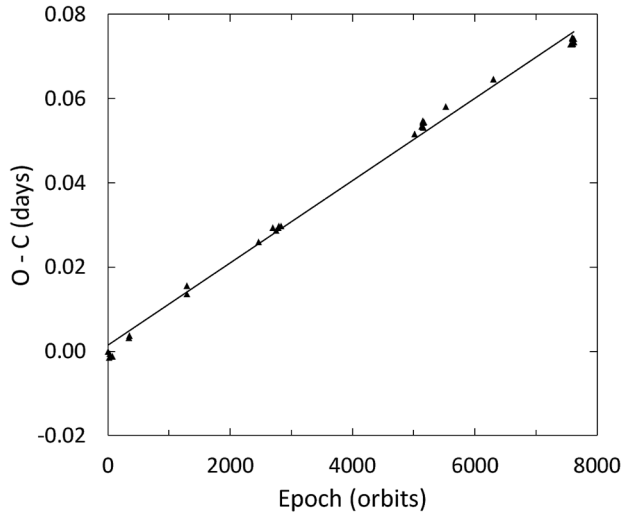

Figure 3. The O–C residuals from Equation 1 with the solid line as the linear ephemeris fit of Equation 2.

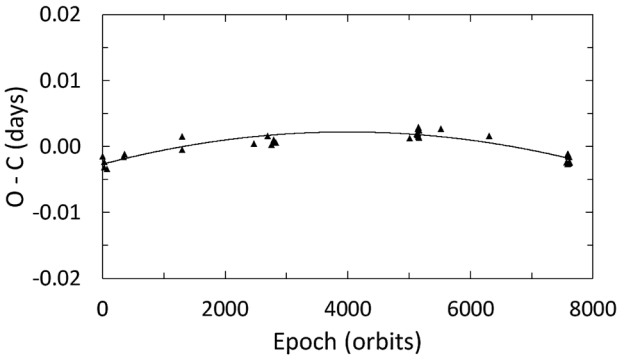

Figure 4. The O–C residuals from Equation 2 with the solid line as the quadratic ephemeris fit of Equation 3.

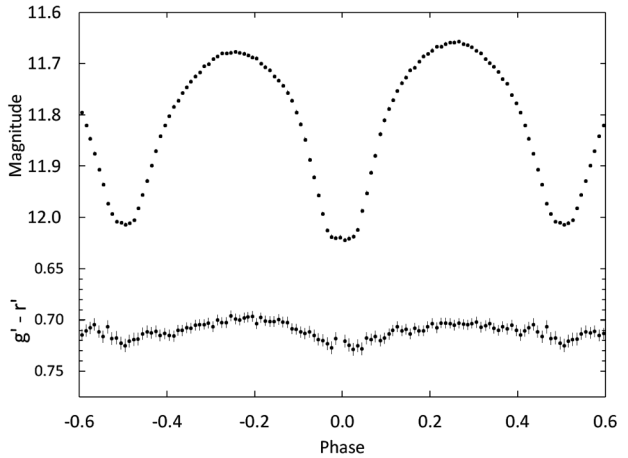

Figure 5. Light curve of all Sloan r'-band observations in standard magnitudes (top panel). The observations were binned with a phase width of 0.01. The errors for each binned point are about the size of the plotted points. The g'- r' colors were calculated by subtracting the linearly interpolated binned Sloan g' magnitudes from the linearly interpolated binned Sloan r' magnitudes.

expected for a contact binary. Using the Bilir *et al.* (2005) transformation equation,

$$(B-V) = \frac{(g'-r') + 0.25187}{1.12431} , \quad (4)$$

gives an observed (B–V) color of 0.850 ± 0.008. The color excess was determined by differencing the observed color and the standard color for a star of spectral type K0. The approximate color excess and interstellar extinction values are $E(B-V) = 0.03 \pm 0.06$ and $A_V = 0.1 \pm 0.2$, respectively. The small values for these two quantities are reasonable given the proximity of V737 Cep to Earth.

4.2. Synthetic light curve modeling

The Sloan g', r', and i' passband data acquired in 2017 were used for light curve modeling. The observations were binned in both phase and magnitude as described in section 4.1. The average number of observations per bin for the g', r', and i' passbands was 12, 9, and 12, respectively. The binned magnitudes were converted to relative flux for modeling. Preliminary fits to the light curves were attained using the program BINARY MAKER3.0 (BM3) (Bradstreet and Steelman 2002). Standard convective parameters were employed in the model with the limb darkening coefficients taken from Van Hamme's (1993) tabular values. A good fit was not possible until a third light contribution was added for all three passbands. There were asymmetries in the light curve as well, but they were not modeled with BM3 in this initial solution attempt. When a good fit was obtained between the synthetic and the observed light curves, the resulting stellar parameters for each passband were averaged. These values were used as the input parameters for computation of a simultaneous three-color light curve solution with the WD program (Wilson and Devinney 1971; Van Hamme and Wilson 1998). The light curve morphology of this star indicates a contact configuration, with the stars having a common convective envelope. The WD program was configured for overcontact binaries (Mode 3). Each binned input data point was assigned a weight equal to the number of observations forming that point. The Method of Multiple Subsets (MMS) was used to minimize strong correlations of parameters (Wilson and Biermann 1976) and the Kurucz stellar atmosphere model was applied. The fixed inputs included standard convective parameters: gravity darkening, $g_1 = g_2 = 0.32$ (Lucy 1968) and albedo value $A_1 = A_2 = 0.5$ (Ruciński 1969). The temperature of the hotter primary star, T_1, was fixed at a 5280 K (see section 4.1). The program calculated linear limb darkening coefficients from tabulated values using the method of Van Hamme (1993). The solution's adjustable parameters include the inclination (i), mass ratio ($q = M_2/M_1$), potential ($\Omega_1 = \Omega_2$), temperature of the secondary star (T_2), the normalized flux for each wavelength (L), third light (l), and phase shift. The best-fit solution parameters with errors are shown in column 2 of Table 3 (Solution 1). The filling-factor in Table 3 was computed using the method of Lucy and Wilson (1979) given by:

$$f = \frac{\Omega_{inner} - \Omega}{\Omega_{inner} - \Omega_{outer}} . \quad (5)$$

For solution 1, $\Omega_{inner} = 5.94$, $\Omega_{outer} = 5.33$, and $\Omega = 5.82$, which gives a fill-out of f = 0.20. Figure 6 shows the normalized light curves overlaid by the synthetic solution curves with the residuals shown in Figure 7.

4.3. Spot model

Low mass, rapidly revolving contact binaries are often magnetically active and thus spotted. The asymmetries seen in the light curves (Figure 6) and in the residuals (Figure 7) are an indication of cool spots or hot regions such as faculae on the star surfaces. The light curves also show an O'Connell effect with Max I ($\phi = 0.25$) brighter than Max II ($\phi = 0.75$), which is also indicative of spotting. The residual plots (Figure 7) show a light loss between orbital phase $\phi = 0.4$ and $\phi = 0.8$, indicating a possible under-luminous region on the larger secondary star. Using the stellar parameters from solution 1, a single cool spot was modeled with BM3. The spot's latitude, longitude, size, and temperature were adjusted until a good fit was obtained between the synthetic and observed light curves. The spot parameters were then incorporated into a new WD solution attempt. The resulting best-fit WD spotted solution parameters are shown in column 3 of Table 3 (Solution 2). Figure 8 shows the final spotted model fit (solid line) overlaid onto the observed light curves with the residuals shown in Figure 9. Solution 2 gave an improved fit with the residuals 2.3 times smaller compared to solution 1. The single large spot on the secondary star was sufficient to model most of the asymmetries in the observed light curves. A graphical representation of solution 2 is shown in Figure 10.

5. Discussion and conclusions

V737 Cep is a W-subtype eclipsing binary with the more massive cooler secondary at a lower surface brightness than its companion. The primary minimum is an occultation. The best-fit spotted WD solution gives a fill-out of 19%, which is consistent with a contact binary. The total eclipses provide the necessary constraints for an accurate determination of the mass ratio (q) in the WD solution (Wilson 1978) (Terrell and Wilson 2005). Provisional absolute stellar parameters can now be calculated using this mass ratio and the secondary star's mass (M_2). M_2 was estimated from the period-mass relation for contact binaries (Gazeas and Stępień 2008):

$$\log M_2 = (0.755 \pm 0.059) \log P + (0.416 \pm 0.024) . \quad (6)$$

The calculated stellar masses are $M_2 = 1.05 \pm 0.09\, M_\odot$ and $M_1 = 0.42 \pm 0.04\, M_\odot$. Kepler's Third Law gives the distance between the mass centers of the two stars, $2.14 \pm 0.05\, R_\odot$. The WD light curve program (LC) computed the stellar radii, surface gravities, and bolometric magnitudes. The mean stellar densities were calculated from the following equations:

$$\bar{\rho}_1 = \frac{0.0189}{r_1^3 (1 + q) P^2} \quad \text{and} \quad \bar{\rho}_2 = \frac{0.0189q}{r_2^3 (1 + q) P^2} , \quad (7)$$

where the stellar radius is normalized to the semi-major axis and P is in days (Mochnacki 1981). All the calculated stellar parameter values are collected in Table 4. A spectroscopic study of this system would provide the radial velocity measurements required to confirm the provisional masses and orbital radii presented here.

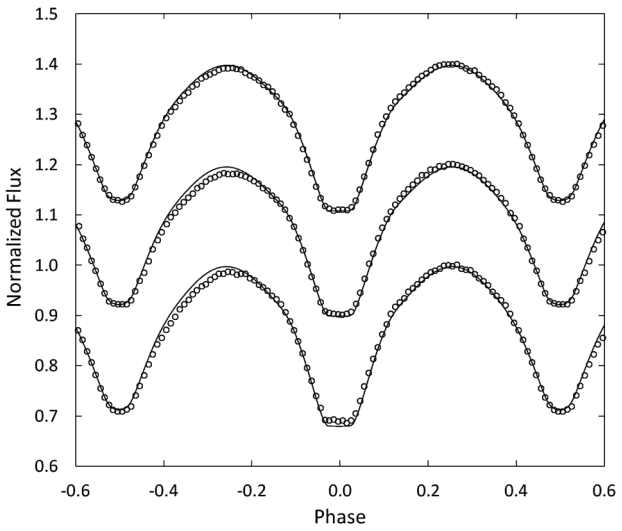

Figure 6. The WD model fit without spots (solid curve) to the observed normalized flux curves for each passband. From top to bottom the passbands are Sloan i', Sloan r', and Sloan g'. Each curve is offset by 0.2 for this combined plot. The best-fit parameters are given in column 2 of Table 3. Error bars are omitted from the points for clarity.

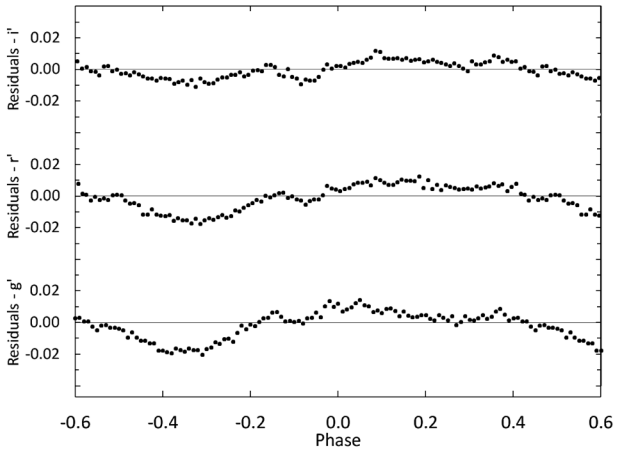

Figure 7. The residuals for the best-fit WD model without spots. Error bars are omitted from the points for clarity.

The (O–C) residuals shown in Figure 4 indicate the orbital period of V737 Cep is decreasing. The quadratic least-squares solution gives the rate of period change as $dP/dt = -8.0\,(4) \times 10^{-7}$ d yr^{-1}, or 6.9 seconds per century. If the decreasing orbital period is the result of a secular period change, then conservative mass exchange is occurring from the larger more massive secondary star to the primary star at a rate of $dM/dt = 6.3\,(2) \times 10^{-7}\, M_\odot$/yr. It is also possible that the period change results from a light-time effect. The (O–C) curve may be a small part of longer sinusoidal ephemeris caused by a third body orbiting the contact binary on a wide orbit. The light curve solution may support the second possibility, given the considerable third-light found, reaching about 37 percent in each passband. A field star could also be responsible for the third-light contribution. Careful examination of the best images

Table 3. Results derived from light curve modeling.

Parameter	*Solution 1 (no spots)*	*Solution 2 (1 spot)*
phase shift	–0.0017 ±0.0002	–0.0036 ±0.0001
filling factor	20%	19%
i (°)	89.8 ± 4	88.1 ± 1
T_1 (K)	[1] 5280	[1] 5280
T_2 (K)	4984 ± 8	4982 ± 6
$\Omega_1 = \Omega_2$	5.82 ± 0.03	5.83 ± 0.02
$q(M_2 / M_1)$	2.50 ± 0.02	2.50 ± 0.01
$L_1 / (L_1 + L_2)$ (g')	0.3918 ± 0.0017	0.3924 ± 0.0007
$L_1 / (L_1 + L_2)$ (r')	0.3679 ± 0.0016	0.3683 ± 0.0007
$L_1 / (L_1 + L_2)$ (i')	0.3581 ± 0.0012	0.3585 ± 0.0006
l_3 (g′)	[2] 0.376 ± 0.005	[2] 0.374 ± 0.003
l_3 (r′)	[2] 0.373 ± 0.005	[2] 0.371 ± 0.003
l_3 (i′)	[2] 0.370 ± 0.004	[2] 0.369 ± 0.003
r_1 side	0.301 ± 0.001	0.303 ± 0.001
r_2 side	0.488 ± 0.004	0.479 ± 0.002
$\sum res^2$	0.14	0.06
Spot Parameters		*Star 2—cool spot*
colatitude (°)		107 ± 14
longitude (°)		318 ± 3
spot radius (°)		24 ± 6
Temp.-factor		0.95 ± 0.02

[1] Assumed.
[2]Third lights are the percent of light contributed at orbital phase 0.25.

The subscripts 1 and 2 refer to the star being eclipsed at primary and secondary minimum, respectively.

Note: The errors in the stellar parameters result from the least-squares fit to the model. The actual uncertainties of the parameters are considerably larger (T_1 and T_2 have uncertainties of about ± 200 K).

Table 4. Estimated absolute parameters for V737 Cep.

Parameter	*Symbol*	*Value*
Stellar masses	M_1 ($M_\odot$)	0.42 ± 0.04
	M_2 ($M_\odot$)	1.05 ± 0.09
Semi-major axis	a ($R_\odot$)	2.14 ± 0.05
Mean stellar radii	R_1 ($R_\odot$)	0.67 ± 0.02
	R_2 ($R_\odot$)	1.01 ± 0.02
Stellar luminosity	L_1 ($L_\odot$)	0.32 ± 0.08
	L_2 ($L_\odot$)	0.57 ± 0.24
Bolometric magnitude	$M_{bol,1}$	6.0 ± 0.3
	$M_{bol,2}$	5.4 ± 0.5
Surface gravity	log g_1 (cgs)	4.40 ± 0.04
	log g_2 (cgs)	4.45 ± 0.04
Mean density	$\overline{\rho}_1$ (g cm^{-3})	1.92 ± 0.06
	$\overline{\rho}_2$ (g cm^{-3})	1.42 ± 0.08

The calculated values in this table are provisional. Radial velocity observations are necessary for direct determination of M_1, M_2, and a.

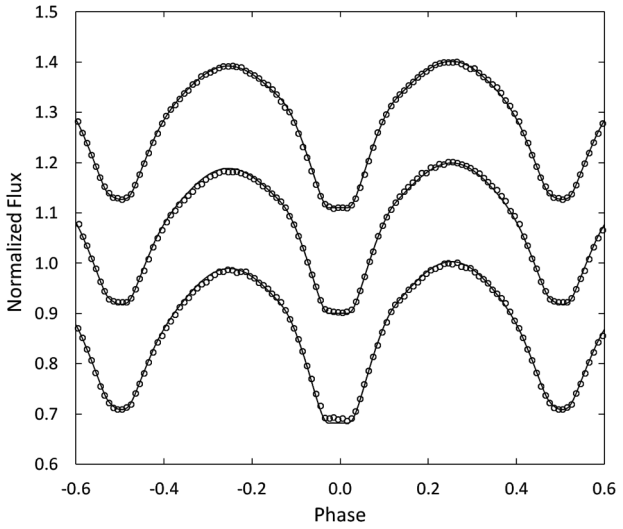

Figure 8. The WD model fit with spots (solid curve) to the observed normalized flux curves for each passband. From top to bottom the passbands are Sloan i', Sloan r', and Sloan g'. Each curve is offset by 0.2 for this combined plot. The best-fit parameters are given in column 3 of Table 3. Error bars are omitted from the points for clarity.

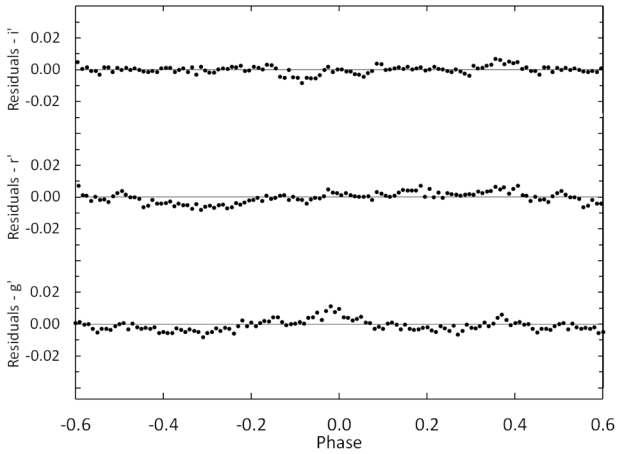

Figure 9. The residuals for the spotted WD model in each passband. Error bars are omitted from the points for clarity.

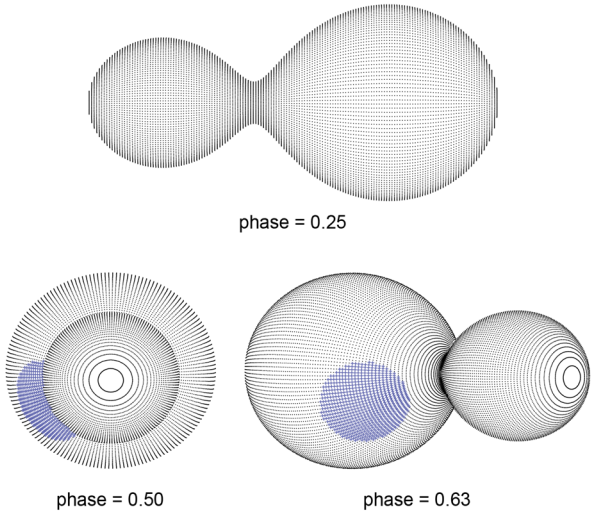

Figure 10. Roche Lobe surfaces of the best-fit wd spot model with orbital phase shown below each diagram.

acquired in this study as well as a Digitized Sky Survey (DSS) image showed no evidence of a field star. Additional precision times of minima spanning several years will be necessary to confirm whether V737 Cep is a trinary system.

6. Acknowledgements

This research was made possible through the use of the AAVSO Photometric All-Sky Survey (APASS), funded by the Robert Martin Ayers Sciences Fund. This research has made use of the SIMBAD database and the VizieR catalogue access tool, operated at CDS, Strasbourg, France. This work has made use of data from the European Space Agency (ESA) mission Gaia (https://www.cosmos.esa.int/gaia), processed by the Gaia Data Processing and Analysis Consortium (DPAC, https://www.cosmos.esa.int/web/gaia/dpac/consortium). Funding for the DPAC has been provided by national institutions, in particular the institutions participating in the Gaia Multilateral Agreement.

References

Bilir, S., Karaali, S., and Tunçel, S. 2005, *Astron. Nachr.*, **326**, 321.

Bradstreet, D. H., and Steelman, D. P. 2002, *Bull. Amer. Astron. Soc.*, **34**, 1224.

Gaia Collaboration: Prusti, T., *et al.* 2016, *Astron. Astrophys.*, **595A**, 1 (Gaia Data Release 1).

Gazeas, K., and Stępień, K. 2008, *Mon. Not. Roy. Astron. Soc*., **390**, 1577.

Gettel, S. J., Geske, M. T., and McKay, T. A. 2006, *Astron. J.*, **131**, 621.

Henden, A. A., *et al.* 2014, AAVSO Photometric All-Sky Survey, data release 9, (http:www.aavso.org/apass).

Hoňková, K., *et al.* 2013, *Open Eur. J. Var. Stars*, No. 160, 1.

Hübscher, J. 2013, *Inf. Bull. Var. Stars*, No. 6084, 1.

Hübscher, J. 2017, *Inf. Bull. Var. Stars*, No. 6196, 1.

Hübscher, J., and Lehmann, P. 2012, *Inf. Bull. Var. Stars*, No. 6026, 1.

Hübscher, J., and Lehmann, P. B. 2013, *Inf. Bull. Var. Stars*, No. 6070, 1.

Hübscher, J., Lehmann, P. B., and Walter, F. 2012, *Inf. Bull. Var. Stars*, No. 6010, 1.

Juryšek, J., *et al.* 2017, *Open Eur. J. Var. Stars*, No. 179, 1.

Kafka, S. 2017, variable star observations from the AAVSO International Database (https://www.aavso.org/aavso-international-database).

Kazarovets, E. V., Samus, N. N., Durlevich, O. V., Kireeva, N. N., and Pastukhova, E. N. 2008, *Inf. Bull. Var. Stars*, No. 5863, 1.

Kukarkin, B. V., and Kholopov, P. N. 1982, *New Catalogue of Suspected Variable Stars*, Nauka, Moscow.

Lucy, L. B. 1968, *Astrophys, J.*, **151**, 1123.

Lucy, L. B., and Wilson, R. E. 1979, *Astrophys, J.*, **231**, 502.

Mirametrics. 2015, Image Processing, Visualization, Data Analysis, (http://www.mirametrics.com).

Mochnacki, S. W. 1981, *Astrophys. J.*, 245, 650.

Nelson, R. H. 2014, *Inf. Bull. Var. Stars*, No. 6092, 1.

Nelson, R. H. 2016, *Inf. Bull. Var. Stars*, No. 6164, 1.

Otero, S., Wils, P., and Dubovsky, P. A. 2005, *Inf. Bull. Var. Stars*, No. 5586, 1.

Pecaut, M. J., and Mamajek, E. E. 2013, *Astrophys. J., Suppl. Ser.*, **208**, 9, (http://www.pas.rochester.edu/~emamajek/EEM_dwarf_UBVIJHK_colors_Teff.txt).

Pickles, A., and Depagne, E. 2010, *Publ. Astron. Soc. Pacific*, **122**, 1437.

Ruciński, S. M. 1969, *Acta Astron.*, **19**, 245.

Terrell, D., and Wilson, R. E. 2005, *Astrophys. Space Sci.*, **296**, 221.

van Hamme, W. 1993, *Astron. J.*, **106**, 2096.

van Hamme, W., and Wilson, R. E. 1998, *Bull. Amer. Astron. Soc.*, **30**, 1402.

Watson, C., Henden, A. A., and Price, C. A. 2014, AAVSO International Variable Star Index VSX (Watson+, 2006–2014; http://www.aavso.org/vsx).

Wilson, R. E. 1978, *Astrophys. J.*, **224**, 885.

Wilson, R. E., and Biermann, P. 1976, *Astron. Astrophys.*, **48**, 349.

Wilson, R. E., and Devinney, E. J. 1971, *Astrophys. J.*, **166**, 605.